Applied Surface Science 594 (2022) 153483

Contents lists available at ScienceDirect

Applied Surface Science

journal homepage: www.elsevier.com/locate/apsusc

Full Length Article

Conformation-dependent thermoelectric power factor of multilayer nanocomposites

You-young Byun [a,1], Junho Jang [b,1], Mario Culebras [c], Byeong-Soo Bae [b], Jung Sang Cho [d], Yong Tae Park [e,*], Chungyeon Cho [a,*]

[a] Department of Carbon Convergence Engineering, College of Engineering, Wonkwang University, Iksan, 54538, Republic of Korea
[b] Wearable Platform Materials Technology Center (WMC), Department of Materials Science and Engineering, Korea Advanced Institute of Science and Technology (KAIST), Daejeon 34141, Republic of Korea
[c] Institute of Materials Science (ICMUV), Universitat de València, Paterna, 46980, Spain
[d] Department of Engineering Chemistry, Chungbuk National University, Chungbuk 361-763, Republic of Korea
[e] Department of Mechanical Engineering, Myongji University, 116 Myongji-ro, Cheoin-gu, Yongin, Gyeonggi-do 17058, Republic of Korea

ARTICLE INFO

Keywords:
Nanocomposites
Weak polyelectrolytes
Thermoelectric
Carbon nanotubes
Multilayer thin films

ABSTRACT

Polyelectrolyte multilayer thin films, assembled by sequentially depositing bilayer (BL) of poly(allyamine hydrochloride) (PAH) and double-walled carbon nanotubes (DWNT) stabilized in polyacrylic acid (PAA) using the layer-by-layer assembly technique, are studied in an effort to establish the relationships between the conformational changes and thermoelectric performances. Controlling the charge density of weak polyelectrolytes with assembly pH conditions gives rise to a different physical, structural, and mechanical properties. The 7.5PAH/3.5 (DWNT-PAA) films exhibit an exponentially-grown thickness behavior due to in-and-out diffusion of the partially charged polyelectrolytes with coiled polymeric conformation, which results in randomly distributed nanotubes within the multilayers. Films made with the same sequences, but with extended polymeric conformation due to high charge density along the polymer chain (PAH at pH 6 and PAA at pH 6.5), show the linear growth behavior with a uniformly oriented nanotube structure and relatively higher elastic modulus. The precise control of the polymeric conformation upon charge density at the nanoscale level significantly affects the thermoelectric performances. A 14 BL 6PAH/6.5(DWNT-PAA) film exhibits an electrical conductivity of 417 S cm^{-1} and Seebeck coefficient of 85 μV K^{-1}. This translates to a power factor of 301 μW m^{-1} K^{-2}, which is 75 times higher than the same films made at pH 7.5/3.5.

1. Introduction

Increasing energy demand and the rapid depletion of non-renewable energy sources based on fossil fuels have led to the global energy crisis. The unprecedented steep increase in energy consumption induces the development of producing eco-friendly energy sources [1–3]. To date, various energy harvesting techniques have been developed using sunlight, electrics, mechanical, and thermal changes (low-grade heat) [4–7]. However, generating electricity from low-grade heat (from sources below 100 °C) remains challenging due to the lack of an effective and cost competitive technology. Thermoelectric (TE) materials that enable direct conversion of heat (e.g., waste heat or heat source from engines, human body, etc.) into electricity have been proved to be effective green energy harvesting systems [3,8,9]. The TE energy conversion efficiency is usually evaluated by the dimensionless figure-of-merit ($ZT = \sigma S^2 T k^{-1}$), where S, σ, k, and T stand for the Seebeck coefficient (or thermopower), electrical conductivity, thermal conductivity, and absolute temperature, respectively. Achieving a high ZT value requires a TE material simultaneously possessing a high S and σ coupled with a low k. Due to the strong conflicting correlations between each physical property, it is very difficult to independently optimize them and simultaneously enhance S and σ [10].

Inorganic semiconductors that are composed of metal alloys including Bi_2Te_3, SiGe, PbTe, and Sb-based materials have been identified as the most commonly used TE materials because of their high performance at a wide range of 400–1200 K [11–14]. In spite of their

* Corresponding authors.
E-mail addresses: ytpark@mju.ac.kr (Y. Tae Park), cncho37@wku.ac.kr (C. Cho).
[1] These authors contributed equally to this work.

https://doi.org/10.1016/j.apsusc.2022.153483
Received 18 February 2022; Received in revised form 9 April 2022; Accepted 22 April 2022
Available online 27 April 2022

excellent TE behaviors, they have several problems such as toxicity, cost-effectiveness, scarcity in the earth's crust, inherent rigidity, and poor processability, which hinders their practical application in the various fields [15–18]. In contrast, conjugated polymers such as polyaniline, polypyrrole, and poly(3,4-ethylenedioxythiophene):poly (styrenesulfonate) have been a promising alternative to inorganic counterparts because of solution-based processability, eco-friendliness, lightweight, and high flexibility [3,9]. Besides, their intrinsically low k (ranging from 0.1 to 1 W m^{-1} K^{-1}) is ideal for improving ZT. However, the power factor ($PF = \sigma^2 S$) of conducting polymers is much lower than that of inorganic TE materials due to their low σ and S [9,19]. Recently, the synergistic combination of low-dimensional carbon nanofillers such as carbon nanotubes, graphene, and graphene oxides and conducting polymers has been exhibited to achieve high PF (>1500 μW m^{-1} K^{-2}) at a relatively low temperature (<500 K) [20,21].

Despite the significant improvements in TE performances of organic materials using various methods including simple mixing, brush-printing, solution-assisted dispersion, in situ chemical polymerization, and polymer emulsion, the PF of organic materials is poor compared to that of inorganic-based composites due largely to the difficulty controlling the film structure and property [22]. A precise control over the film's architecture and uniform arrangement of carbon nanoparticles in the polymer matrix is necessary to produce a novel 3D network that can promote efficient charge transport [23]. In this regard, the layer-by-layer (LbL) method is an effective alternative to create the hybrid composites where carbonaceous materials are uniformly incorporated into a layered nanostructure. LbL assembly is one of the most effective methods for preparing well-defined multilayer thin films with nanometer-scaled thickness precision and highly ordered internal structure [3,24]. The polymeric nanocomposites are prepared by sequentially immersing a charged substrate into aqueous solutions containing complementarily functionalized materials such as nanoparticles, inorganic nanoplates, dendrimers, and biomaterials onto any geometric surfaces [25–27]. The multilayer formation is mainly driven by electrostatic interactions between oppositely charged species, but assemblies based on hydrogen bonding, hydrophobic interaction, covalent bonds, and donor/acceptor interactions have also been investigated [24]. The properties of LbL assembly can be simply tailored by controlling temperature, assembly pH conditions, molecular weight, types of polymers used and deposition time [28,29]. Furthermore, the multilayer thin films have been shown to be capable of reorganization even after assembly upon external stimuli such as humidity, electric potential, pH, ionic strength, and solvent [30].

In regard to polymeric substrates, the self-assembled LbL structures have been extensively exploited to develop advanced functional materials in various fields including gas barrier, self-cleaning materials, biosensors, flame retardant, and tissue engineering [31,32]. In recent years, electrostatically layered nanocomposites have been studied for organic TE materials because a continuous 3D conjugated network created by the sequential self-assembly of conducting polymers and carbon-based materials leads to synergistically improved TE performances [2,9,22]. Of particular interest is the intricate control of weak polyelectrolytes-based LbL films that can be induced by changes in the assembly pH. Previous reports have shown that the variation of charge density in polymer chains can produce distinct structure, physical/mechanical properties, and film composition [33]. Various strategies have been attempted to enhance the TE properties via chemical doping, quantum confinement, carrier filtering, and engineering the electronic band structure [34–36]. However, relatively little works have been done on the effects of conformational changes of weak polyelectrolytes on TE behaviors.

Here, we demonstrate the structural tailoring of LbL films containing pH-sensitive polyelectrolytes (poly(allyamine hydrochloride) (PAH) and polyacrylic acid (PAA)) and double-walled carbon nanotubes (DWNT) by changing assembly pH conditions for developing organic nanocomposites with high TE performances. The LbL thin films assembled with weak polyelectrolytes exhibit tunable thickness, composition ratio, and structures by controlling the degree of ionization of polyelectrolytes with the pH or ionic strength of the assembly solution [37–39]. In this work, two different assembly pH conditions resulted in different physical and mechanical properties and morphologies, which ultimately affected the TE properties. PAH/DWNT-PAA bilayer (BL) films assembled at pH 7.5/3.5 showed a loosely packed nanostructure with randomly oriented nanotubes within the multilayers thin films, so there was little benefit in TE performances. The same multilayers deposited at pH 6/6.5 resulted in densely packed nanostructure where the TE properties were enhanced through the multidimensional conjugated network. A 14 BL thin film (~340 nm thick) of PAH/DWNT-PAA deposited at pH 6/6.5 exhibited an electrical conductivity of 417 S cm^{-1} and Seebeck coefficient of 85 μV K^{-1}, translating to a power factor of 301 μW m^{-1} K^{-2}. This is 75 times higher relative to that of the same films assembled at pH 7.5/3.5.

2. Materials and methods

2.1. Materials

Double-walled carbon nanotubes (DWNT) (XB type, diameter ~ 3 nm and length 1 μm, purity ≥ 95%) were purchased from Continental Carbon Nanotechnology Inc. (Houston, TX). Poly(allyamine hydrochloride) (PAH) (MW = 70,000 g mol^{-1}) and poly(acrylic acid) (PAA) (MW = 100,000 g mol^{-1}) were purchased from Sigma-Aldrich (St. Louis, MO, USA). All chemicals were used as received unless otherwise stated. The uniformly dispersed nanotubes were achieved by manually grinding 0.03 wt% DWNT in distilled (DI) water containing 0.1 wt% PAA using a mortar and pestle for 15 min. These suspensions were then sonicated using a Bandelin Sonopuls tip-sonicator for 1 h to ensure stable dispersions. The stabilized DWNT suspensions in PAA solutions were subjected to centrifuge (4,000 rpm for 20 min) and the supernatant was decanted. The pH of PAH and DWNT-PAA solutions was adjusted using 0.1 and 1 M HCl or NaOH purchased from Sigma-Aldrich (St. Louis, MO, U.S.A).

2.2. Substrates

A poly(ethylene terephthalate) (PET) film was purchased from FilmBank (Gyeonggi-do, Korea). In order to create a negative surface charge and improve adhesion of the first PAH layer, corona treatment was performed on the cleaned PET substrates with a hand-held corona treater (BD-20C, Electro-Technic Products Inc., Chicago, IL). Single-side-polished silicon wafers (University Wafer, South Boston, MA) were used as the substrate for profilometer, atomic force microscopy (AFM), scanning electron microscopy (SEM), and ultraviolet photoelectron spectroscopy (UPS). Si-wafers were rinsed with DI water, acetone, and then DI water prior to use. Polypropylene (PP) sheets with a thickness of 1.6 mm were obtained from AlfaAesar (WardHill, MA, USA), and used for thermogravimetric analysis (TGA). Corona treatment was omitted on PP to induce the weak adhesion between polyelectrolytes and substrates. A quartz slide was used for Fourier-transform infrared spectroscopy (FT-IR) analysis. The increased mass per layer was detected by using a quartz crystal microbalance (QCM) with polished Ti/Au crystals of 5-MHz resonant frequency (Maxtek, Inc., Cypress, CA). The crystal was rinsed and left dry to stabilize for 3 min between each deposition, which reduces water's contribution to the QCM mass gains.

2.3. Layer-by-layer assembly

The multilayer thin films were assembled with a Multi Dip Coater robot (Hantech Co., Daejeon, Korea) on Si-wafers, quartz, and PET as substrates. Each cleaned substrate was submerged first into the positively charged PAH solution for 5 min along with a series of three rinse baths of DI water for 20 sec each to remove physically absorbed excess PAH. The PAH coated substrate was dipped into DWNT-PAA mixtures

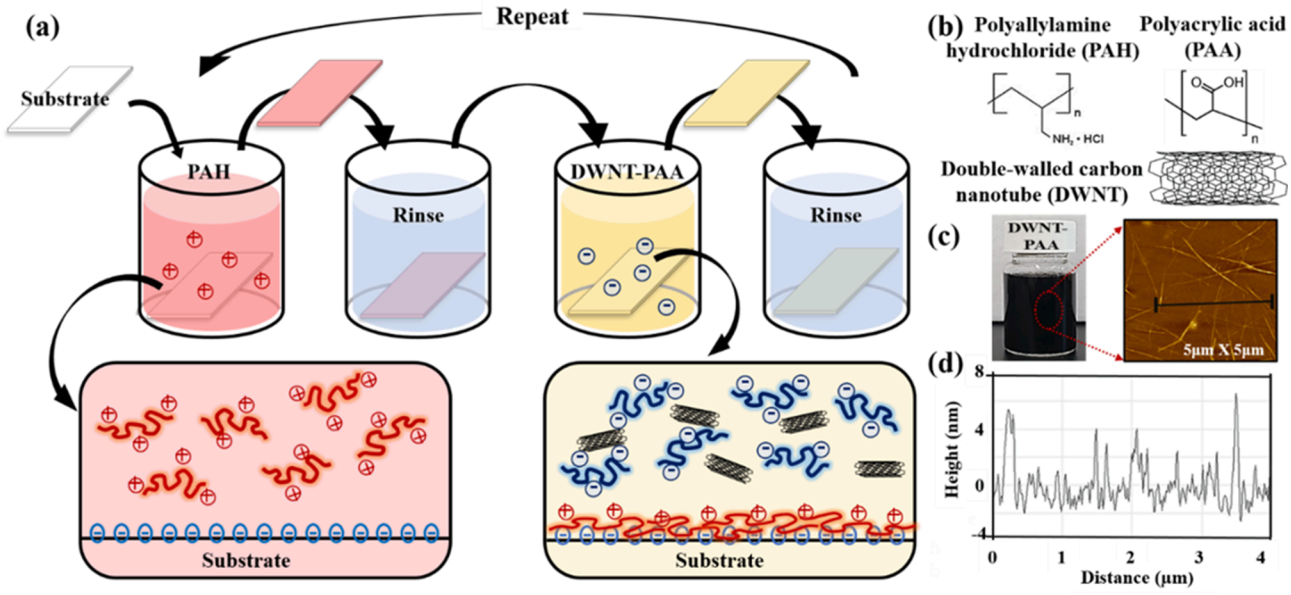

Fig. 1. (a) Schematic illustration of the layer-by-layer deposition process for the preparation of PAH/DWNT-PAA. (b) Chemical structures of polyelectrolytes and carbon nanotubes used in this study. (c) Photograph of DWNT suspensions stabilized by PAA in water and AFM height image and (d) height profile of nanotubes in the corresponding suspension cast onto Si-wafer.

for 5 min, followed by three rinse baths for 20 sec each, which results in one bilayer (BL) of PAH/DWNT-PAA. After the first BL was assembled, subsequent cycles were achieved by repeating 2 min deposition while the rinsing steps kept the same as the initial BL. For the remainder of this paper PAH/DWNT-PAA will be denoted as XPAH/Y(DWNT-PAA), where X and Y are the pH value of each solution. For instance, 7.5PAH/3.5(DWNT-PAA) refers to a sample in which the deposition pH of the PAH and DWNT-PAA solutions is adjusted to 7.5 and 3.5, respectively. The assembled multilayer thin films were dried at room temperature and stored in a desiccator prior to measurements.

2.4. Characterization

Thickness of the thin films on Si-wafers was conducted with a NanoMap-PS stylus contact profiler (AEP Technology, Santa Clara, USA). Five measurements were taken on three different samples and the measurements were averaged to represent the reported values. A QCM200 (Stanford Research Systems, Inc., CA) was used to analyze the adsorbed mass of each layer. Surface topography of thin films was obtained by using AFM (Nanostation Surface Imaging Systems, Germany) in the non-contact mode at a scan rate of 1 Hz in the air. Top-view images of the multilayer were captured with an S-4800 field emission scanning electron microscope (FE-SEM, Hitachi, Japan). For the examination of cross-sectional structure, LbL assemblies were fractured with a diamond cutter after freezing them in liquid nitrogen for a few minutes. TGA experiments on a PerkinElmer TGA 8000 (Ohio, USA) were performed with a heating ramp of 10 °C min^{-1} up to 700 °C under nitrogen atmosphere. FT-IR spectra were recorded at room temperature using an FT-IR 680 plus (JASCO). The UV–vis spectroscopy of the LbL films was carried out in absorption mode using a Shimadzu UV-1900 spectrophotometer (Shimadzu Corporation, Tokyo, Japan). Elastic modulus was analyzed using an ultra-nanoindentation system (UNHT3, Anton Parr, Switzerland) with a sphero-conical (2 μm tip radius, 90° cone angle) indenter tip. Ultraviolet photoelectron spectroscopy (UPS) profiles of the multilayer thin films deposited on gold-coated Si-wafers were obtained with a Sigma Probe (Thermo VG Scientific, USA). The work function was calculated from the difference between excited photon energy of 21.2 eV (He I emission line) and Fermi level energy (0 eV).

2.5. Thermoelectric measurements

Sheet resistances on 5 X 10 mm thin films deposited on PET substrates were measured by using a four-point probe (CMT-100S, Advanced Instrument Technology) equipped with 0.4 mm probe tip diameter and a separation of 0.72 mm between each tip. The Seebeck coefficient of the samples (10 X 30 mm) was determined by using a custom-built four-point probe setup where electrical voltage ($\Delta V = V_{cold} - V_{hot}$) and temperature difference ($\Delta T = T_{hot} - T_{cold}$) were measured by two copper wires and two T-type thermocouples, respectively. The in-plane thermoelectric voltage across the LbL films induced by the temperature differentials between −7 and 7 K around room temperature was recorded by a computer equipped with LabVIEW software. After multiple measurements of thermovoltages and temperature differences, the Seebeck coefficient of each film was derived from the slopes of the straight-line fits of the ΔV–ΔT plots with a correlation coefficient greater than 0.99. The reported electrical conductivity and Seebeck coefficient in Fig. 4 are the average values of five measurements on three independent samples. Hall effect measurements with the Van der Pauw geometry (20 X 20 mm) were conducted at room temperature to determine the electronic carrier concentration and mobility. An external magnetic field of 1 T and a current of 100 μA were applied using an Ecopia HMS-3000 measurement system with ohm contact established using Au electrodes. The load voltage (V) and load current (I) were obtained by varying the resistance of load resistor. The output power (P) was calculated by using the formula $P = V \bullet I$.

3. Results and discussion

Fig. 1a shows the layer-by-layer (LbL) process used to assemble two different bilayer (BL) systems (7.5PAH/3.5(DWNT-PAA) and 6PAH/6.5 (DWNT-PAA)), differentiated by assembly pH conditions. Fig. 1b shows the chemical structures of each component used in this study. Multilayer formation involves the sequential adsorption of a substrate into the positively charged PAH solution and an aqueous suspension containing DWNT in negatively charged PAA. The DWNT nanoparticles, stabilized by anionic PAA, are enveloped by the PAH and PAA during deposition. An optical image of DWNT in PAA polymer solutions showed that electrostatic repulsions provided by wrapping the DWNT with anionic

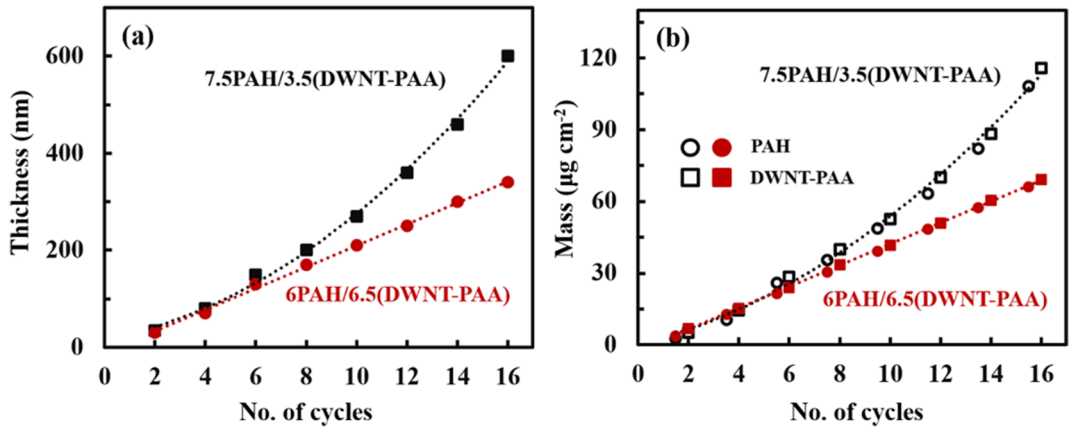

Fig. 2. (a) Thickness and (b) mass growth of 7.5PAH/3.5(DWNT-PAA) and 6PAH/6.5(DWNT-PAA) thin films as a function of the number of layers deposited.

PAA led to a stable colloidal dispersion in water after sonication and centrifugation (Fig. 1c). Atomic force microscope (AFM) images of drop-casting from dilute solutions confirmed a homogeneous dispersion of DWNT in PAA without significant aggregation. The AFM height profile revealed that the individual DWNT is around 2–3 nm thick (Fig. 1d), suggesting fully exfoliated these nanotubes.

3.1. Film growth

Film growth of two different PAH/DWNT-PAA pH combinations (7.5PAH/3.5(DWNT-PAA) and 6PAH/6.5(DWNT-PAA)) was measured with a profilometer after every two BLs were deposited on a Si-wafer, as shown in Fig. 2a. Growth behavior of an LbL film was shown to be strongly governed by charge density of weak polyelectrolytes by altering the pH value of deposition solution [40]. 6PAH/6.5(DWNT-PAA) films grew linearly at a rate of 21 nm per BL. On the other hand, the thickness of 7.5PAH/3.5(DWNT-PAA) multilayers increased exponentially, achieving a thickness of 600 nm at 16 BL. The variation of growth behavior with pH conditions is thought to be caused by two factors: (1) conformational changes of polyelectrolytes and (2) "in-and-out" diffusion during deposition process. The charge density of weak polyelectrolytes can be simply controlled by the pH of the assembly solution, which ultimately affects chain conformation [41]. When assembled at pH 6 and 6.5 for PAH and DWNT-PAA, respectively, both polyelectrolytes are fully charged with expanded conformation due to intrasegmental repulsion, resulting in a highly ionically cross-linked (NH_3^+ … COO^-) film comprised of molecularly thin layers. The pKa, specific pH value at which half of functional groups of polyelectrolytes are ionized, of PAH and PAA is reported to be ~ 9 and ~ 5, respectively. At pH 7.5 for PAH and 3.5 for DWNT-PAA, both the partially charged PAH and PAA have a lower charge density, taking on a loop-rich conformation due to intramolecular van der Waal attractions and lack of electrostatic repulsion [42]. The charge density variation of the two LbL films was investigated by using FT-IR (Fig. S1). The ratio of the peak intensity of ionized acid groups to neutral COOH in the 7.5PAH/3.5 (DWNT-PAA) films is lower, indicating that the degree of ionization of PAA in the 6PAH/6.5(DWNT-PAA) films is higher than that of the films assembled at pH 7.5/3.5.

Furthermore, these coiled polyelectrolytes highly interdiffuse to compensate for the charge reversal of the film's surface during the film

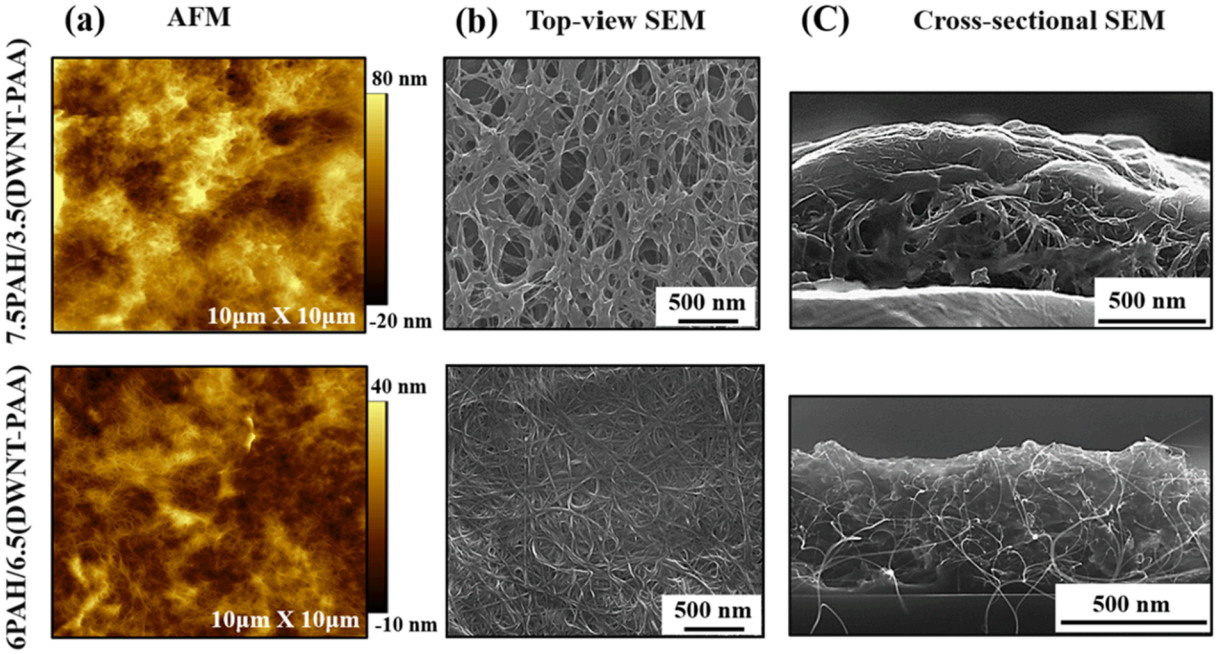

Fig. 3. (a) AFM height images, (b) top-view SEM images, and (c) cross-sectional SEM images of PAH/DWNT-PAA bilayer films assembled with different pH conditions.

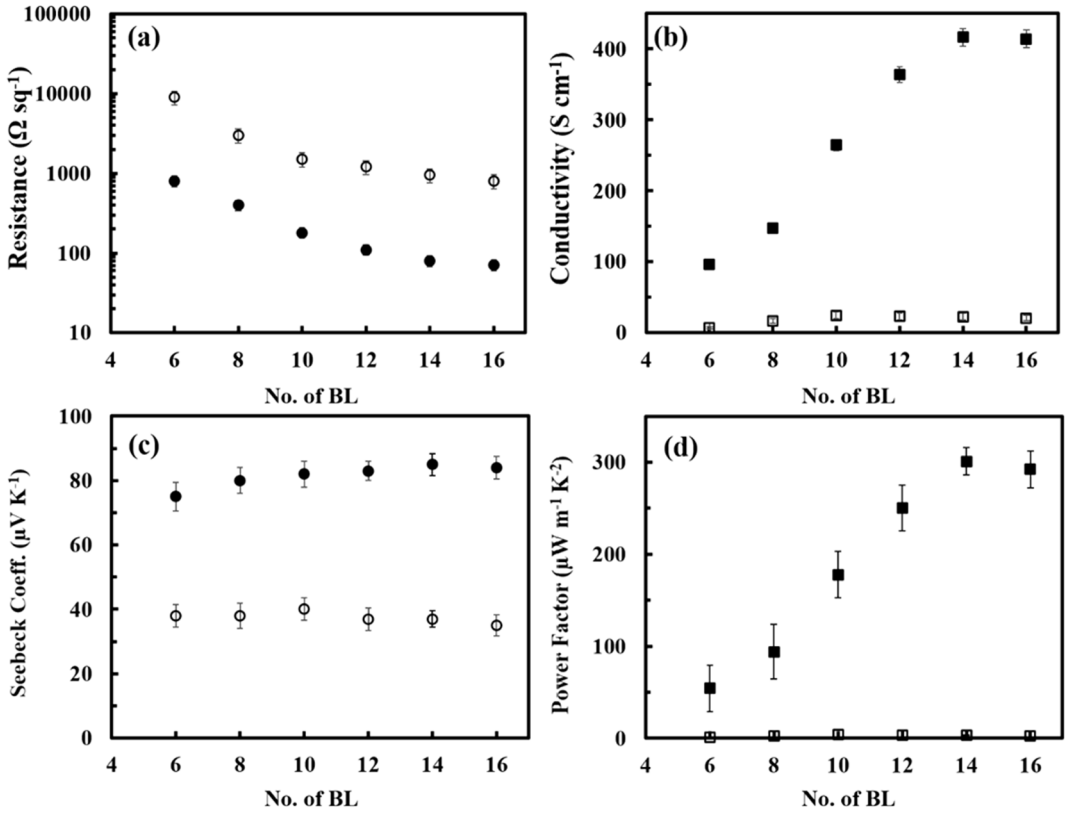

Fig. 4. (a) Sheet resistance, (b) electrical conductivity, (c) Seebeck coefficient, and (d) power factor of 7.5PAH/3.5(DWNT-PAA) (open circle and square) and 6PAH/6.5(DWNT-PAA) (filled circle and square) as a number of bilayers deposited on a PET substrate. Full analysis of electrical conductivity and power factor of 7.5PAH/3.5(DWNT-PAA) alone are shown (Fig. S7, Supporting Information).

assembly, resulting in the dramatic increase in thickness. The thickness of DWNT-containing films is thicker relative to that of the LbL films with no nanotubes deposited, meaning that the PAH and PAA have enveloped the carbon nanofillers (Fig. S2). In the 7.5PAH/3.5(DWNT-PAA) systems, inclusion of the nanotubes did not prevent exponential growth behavior. This implies reptation and permeation of PAH and PAA between the nanotubes layers in the aqueous deposition environment, allowing polyelectrolytes to diffuse in and out during assembly, as reported with other carbon and inorganic materials [43–45].

The mass increase was measured with the number of layers deposited using a quartz crystal microbalance (QCM), as shown in Fig. 2b. Similar to the thickness growth, QCM data confirmed the linear growth trend for 6PAH/6.5(DWNT-PAA) and exponential trend for 7.5PAH/3.5(DWNT-PAA). Based on film thickness (from profilometer) and mass (from QCM analysis), the densities of 6PAH/6.5(DWNT-PAA) and 7.5PAH/3.5(DWNT-PAA) films are calculated to be 2.03 and 1.78 g cm^{-3}, respectively. The higher density of the 6PAH/6.5(DWNT-PAA) films is presumably due to a more tightly packed structure. In an effort to obtain the weight fraction of DWNT deposited in the films, TGA was carried out at a heating rate of 10 °C min^{-1} in a nitrogen atmosphere (Fig. S3). TGA analysis revealed that a greater amount of nanotubes is deposited in the 6PAH/6.5(DWNT-PAA) films. When taken together, QCM and TGA results provide the composition of each component. For 6PAH/6.5(DWNT-PAA), the concentrations of PAH, PAA, and DWNT were determined to be 34.5, 44.1, and 21.4 wt%, respectively. The 7.5PAH/3.5(DWNT-PAA) films contained 44.8, 45.1, and 10.1 wt% for PAH, PAA, and DWNT, respectively. The DWNT concentration in the 7.5PAH/3.5(DWNT-PAA) films decreases with increasing the number of assembly cycles because both the partially ionized PAH and PAA are contributing to the exponential growth.

3.2. Film structure

In an effort to visualize the surface morphology and interior structure, AFM and SEM analysis on the LbL films were performed. The AFM images of both 7.5PAH/3.5PAA and 6PAH/6.5PAA films with no nanotubes deposited showed similar morphologies with continuous and smooth surfaces (Fig. S4). The LbL films incorporated with DWNT clearly revealed that the surface is fully covered with a large quantity of nanotubes, as shown in Fig. 3a. It is clear that the 6PAH/6.5(DWNT-PAA) films had homogeneously distributed individual DWNT and their bundles on the surface, while the 7.5PAH/3.5(DWNT-PAA) films showed extensively aggregated nanotubes. Much like with AFM analysis, the surface and cross-sectional SEM images of the LbL films without nanotubes displayed featureless structures (Figs. S5 and S6). The morphology from the SEM images of LbL films in the presence of DWNT was similar, but the 7.5PAH/3.5(DWNT-PAA) films contained much thicker bundles relative to those of 6PAH/6.5(DWNT-PAA) (Fig. 3b). Top-view SEM images of the 7.5PAH/3.5(DWNT-PAA) films represented highly aggregated bundles of nanotubes with porous surface structures. On the other hand, the surface of 6PAH/6.5(DWNT-PAA) films had excellent coverage of multiple nanotube networks. In addition, the cross-sectional SEM micrographs showed that multiple nanotubes are prevalent and homogeneously deposited in the interior of the 6PAH/6.5(DWNT-PAA) films (Fig. 3c).

The difference in the surface morphology and internal structures between these two LbL films is likely due to the assembly pH conditions. The partially charged polyelectrolytes (PAH at pH 7.5 and PAA at pH 3.5) not only adsorb onto the surface but also interpenetrate into inner layers for interactive charge overcompensation between each deposition, which causes the already deposited nanotubes to be randomly distributed in the films [42]. In contrast, mutual charge compensation with a 1:1 stoichiometry of a flattened conformation occurs in 6PAH/6.5

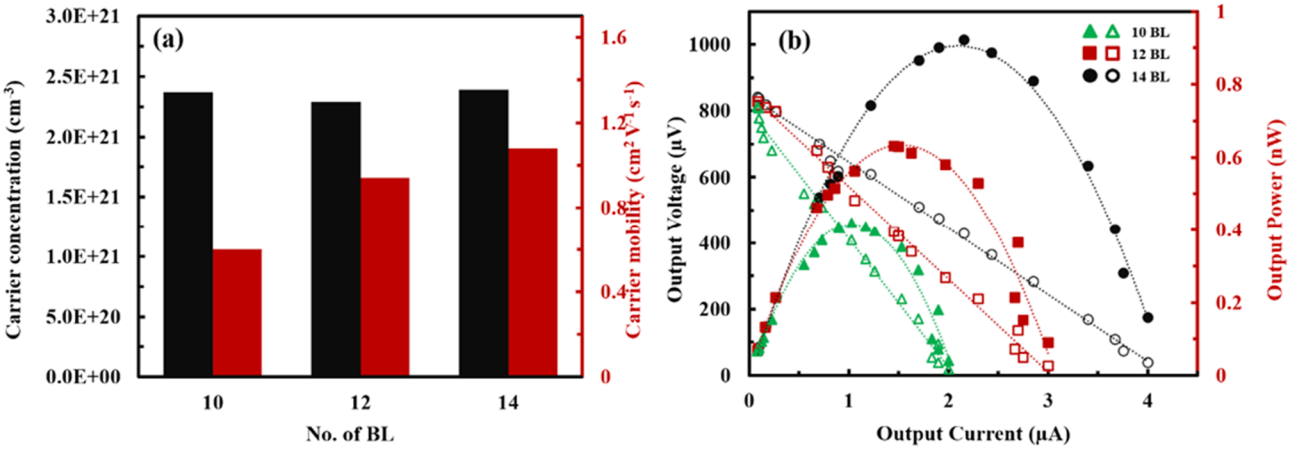

Fig. 5. (a) Carrier concentration and carrier mobility of the 6PAH/6.5(DWNT-PAA) films from Hall Effect measurements. (b) Output voltage (open symbols) and output power (closed symbols) of the 6PAH/6.5(DWNT-PAA) films as a function of bilayers deposited at a temperature difference of 9.8 K.

(DWNT-PAA), preserving the densely packed nanotubes structure that had been formed during the LbL process. Both AFM and SEM analysis showed that the film's structure containing carbon nanotubes can be simply controlled by altering the charge density along the polymer chains. Due to the fact that the electrical property of nanocomposites is highly dependent on the degree of effective interconnection between nanotubes, continuous electrically conductive pathways in the 6PAH/6.5(DWNT-PAA) films are expected to produce higher thermoelectric performances [37,46,47].

3.3. Thermoelectric performance

Electrical properties of PAH/DWNT-PAA systems were studied to determine how different pH assembly conditions affect performance. We have measured the sheet resistance of the LbL films, deposited on an insulating poly(ethylene terephthalate) (PET) substrate, using a four-point probe station as a function of BL deposited at room temperature. The sheet resistance of both LbL systems decreased as more layers were added because of increased connectivity of the DWNT with thickness (Fig. 4a). The sheet resistance of the 7.5PAH/3.5(DWNT-PAA) films gradually decreased from 9 kΩ sq^{-1} at 6 BL to 820 Ω sq^{-1} at 16 BL. More dramatic decrease in sheet resistance occurred in the 6PAH/6.5(DWNT-PAA) films, exhibiting 790 Ω sq^{-1} at 6 BL to 70 Ω sq^{-1} at 14 BL. Electrical conductivity was calculated directly by taking the inverse of multiplying the sheet resistance and layer thickness. The electrical conductivity of the 7.5PAH/3.5(DWNT-PAA) films increased up to 24.7 S cm^{-1} at 10 BL, and then decreased to 20.8 S cm^{-1} at 16 BL (Fig. 4b and Fig. S7a). The 6PAH/6.5(DWNT-PAA) films exhibited that electrical conductivity increased modestly with thickness (96 S cm^{-1} at 6 BL up to 417 S cm^{-1} at 14 BL), suggesting that a more conjugated carbon network for electron transfer is created upon the layers deposited. Then, the electrical conductivity reached a stable value of about 410 S cm^{-1} with further addition of layers beyond 16 BL, implying that the percolation network of DWNT is fully realized in the 6PAH/6.5(DWNT-PAA) films.

The Seebeck coefficient as a number of BLs deposited is shown in Fig. 4c. The 7.5PAH/3.5(DWNT-PAA) films showed the Seebeck coefficient in the range of 35 to 40 μV K^{-1}. The Seebeck coefficient in the 6PAH/6.5(DWNT-PAA) films increased up to 85 μV K^{-1} at 14 and then levelled out beyond 16 BL. The 6PAH/6.5(DWNT-PAA) films exhibited higher Seebeck coefficient relative to that of films made with partially charged polymers. This is not an unexpected result because more efficient carrier transport is formed in the 6PAH/6.5(DWNT-PAA) films. The power factor (*PF*) was calculated as the product of the Seebeck coefficient squared and electrical conductivity, as shown in Fig. 4d. The 7.5PAH/3.5(DWNT-PAA) assemblies exhibited an increased *PF* from 1.07 μW m^{-1} K^{-2} at 6 BL to 3.95 μW m^{-1} K^{-2} at 10 BL, but adding more layers reduced the *PF* down to 2.55 μW m^{-1} K^{-2} at 16 BL (Fig. S7b). Interestingly, the *PF* was enhanced dramatically by tuning assembly pH conditions. The *PF* of the 6PAH/6.5(DWNT-PAA) films increased with thickness in a similar manner to electrical conductivity (Fig. 5(b)). A maximum *PF* of the 6PAH/6.5(DWNT-PAA) films was 301 μW m^{-1} K^{-2} at 14 BL, which is 75 times as large as the multilayers deposited at pH 7.5 and pH 3.5 for PAH and DWNT-PAA, respectively.

It is noteworthy that both electrical conductivity and Seebeck coefficient increased together with the number of layers deposited (Fig. 4b and 4d), indicating that the interdependence of the TE behavior was decoupled. This simultaneous rise is a unique TE behavior, considering that the conventional inorganic TE materials suffer from adverse correlation in physical variables [48,49]. In order to elucidate these decoupled TE properties, carrier concentration and carrier mobility were analyzed by using Hall effect measurements in van der Pauw geometry at room temperature. The difference in carrier concentration between 7.5PAH/3.5(DWNT-PAA) and 6PAH/6.5(DWNT-PAA) films is less than 60%, with the latter being higher (Fig. 5a and Fig. S8). However, the 6PAH/6.5(DWNT-PAA) films had two orders of magnitude higher mobility, as compared to the counterpart ones. This large increase in carrier mobility contributes to the high TE performance. The carrier mobility at 14 BL of the 6PAH/6.5(DWNT-PAA) films increased by a factor of 1.8 relative to 10 BL, while the carrier mobility showed little change from 2.37 × 10^{21} cm^{-3} at 10 BL to 2.39 × 10^{21} cm^{-3} at 14 BL. This indicates that the decoupled TE properties were driven more by carrier mobility rather than electrical concentration.

Practical applications of these materials to effectively harvest energy from wasted heat requires TE power generator, regardless of the calculated *ZT*. Output voltage and power output measurements of the 6PAH/6.5(DWNT-PAA) films (5 X 15 mm) were performed, as shown in Fig. 5b. Both the output voltage and maximum output current increased proportionally with the number of layers deposited. The maximum output power generated in the 14 BL 6PAH/6.5(DWNT-PAA) films was 0.92 nW at a temperature difference of 9.8 K. Although this power output is low for most TE applications, modules based on the present films do not have the limitations to be applicable in large areas and they could be utilized for low power devices provided the thermocouples consisting of hundreds of the films are supplied with a sufficient ΔT [50].

3.4. Highly-Tunable thermoelectric behavior

The difference in the thermoelectric properties of two LbL systems assembled from the same components is attributed to different nanostructures created by pH-sensitive polymeric conformation of the weak polyelectrolytes. Tailoring the charge density of weak polyelectrolytes

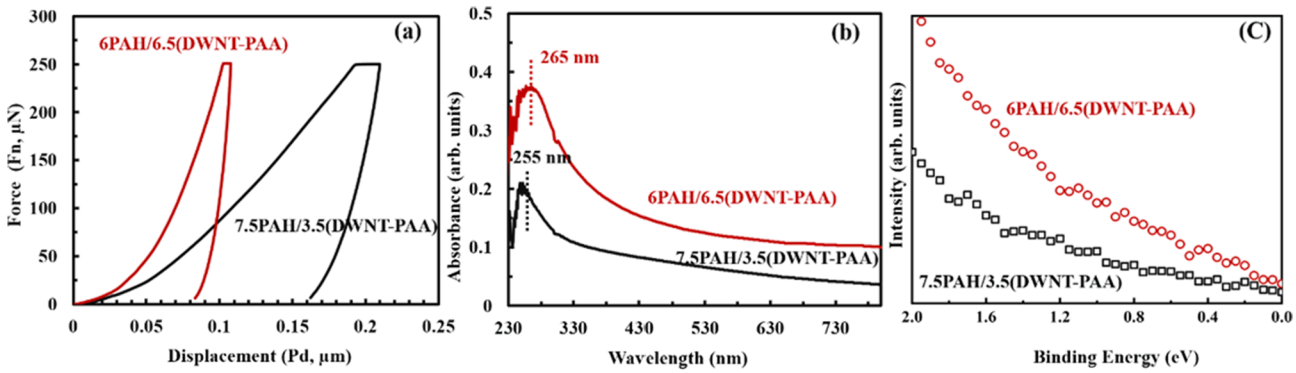

Fig. 6. (a) Indentation force as a function of displacement, (b) UV–vis spectra, and (c) UPS spectra of PAH/(DWNT-PAA) thin films assembled with different pH conditions.

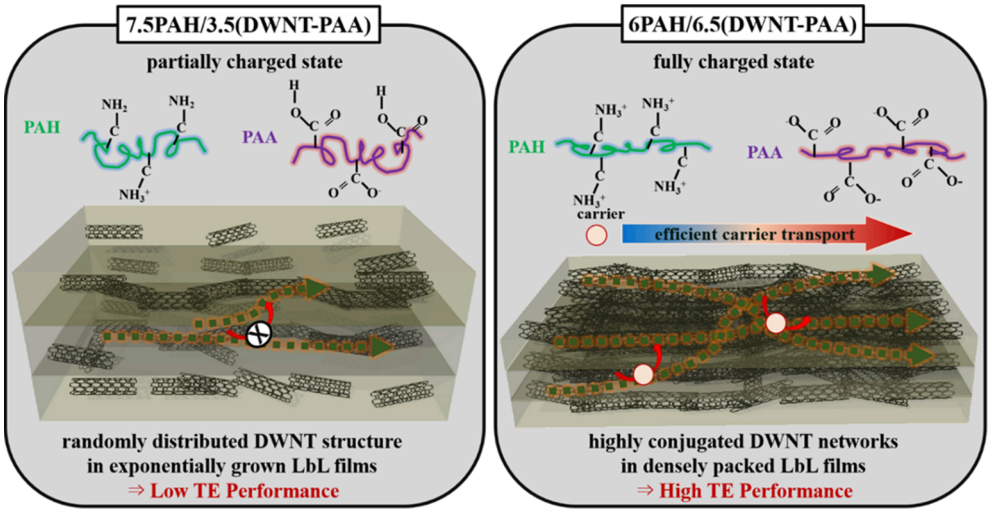

Fig. 7. Molecular structures of PAH and PAA at different charge densities and schematic illustration of the DWNT network in the PAH/DWNT-PAA films created at different assembly pH conditions.

by varying the assembly pH conditions ultimately leads to two extreme cases in film's growth behavior. In the LbL films made from polymers with low charge (PAH at pH 7.5 and PAA at pH 3.5), a greater amount of intrinsically non-conducting polymers is deposited relative to DWNT during the LbL process, and in-and-out diffusion of weakly charged polyelectrolytes causes the π–π conductive nanotube structure to be disrupted. The nanoindentation results (Fig. 6a), obtained from 1 μm thick films assembled at different pH, showed that the elastic modulus of 6PAH/6.5(DWNT-PAA) is 2.3 GPa, which is more than 3 times as large as that (0.7 GPa) of 7.5PAH/3.5(DWNT-PAA). The higher mechanical property in the films assembled with PAH at pH 6 and DWNT-PAA at pH 6.5 is due to a densely packed nanostructure where carbon nanotubes that have been enveloped by highly charged polyelectrolytes with extended conformation are uniformly aligned within the films.

The observation of ordered carbon nanotube structures assembled at the pH corresponding to a high degree of ionization was confirmed by UV–vis absorbance measurements, as shown in Fig. 6b. The characteristic absorbance peak of DWNT in the 3 BL 6PAH/6.5(DWNT-PAA) films was red-shifted by 10 nm in comparison to that of the respective pH 7.5/3.5 ones. This shift toward higher wavelength implies ordered nanotube arrangements, strengthening the π-π conjugation pathways and hence increasing carrier transport between DWNT junctions within the nanocomposites [2,9]. The assembly pH-dependent behavior of TE performances was further analyzed on 1 μm thick films by using ultraviolet photoelectron spectroscopy (UPS). According to Mott's formalism, $S(E,T) = \frac{\pi^2}{3}\cdot\frac{k^2T}{q}\cdot\left(\frac{\partial \ln(\sigma(E))}{\partial E}\right)_{E=E_f}$, the Seebeck coefficient is closely related to the density of states (DOS) slope at the Fermi level; a steeper slope results in a larger Seebeck coefficient [51]. Fig. 6c exhibits that the 6PAH/6.5(DWNT-PAA) films had a steeper slope, implying that highly ordered nanocomposites have larger Seebeck coefficient. By using UPS spectra, the highest molecular orbital (HOMO) and work function of 14 BL LbL films were calculated (Table S1). The 6PAH/6.5(DWNT-PAA) films exhibited a larger work function with an upward shift of HOMO edge in comparison with 7.5PAH/3.5(DWNT-PAA). The larger energy difference between HOMO and work function means a lower Fermi level, indicating stronger p-type conversion that leads to a higher Seebeck coefficient [52–55].

Based on the above results, the scheme on carrier transport mechanism is postulated in Fig. 7. As studied previously, weak polyelectrolytes (*i.e.,* such as PAH and PAA), enable the creation of a wide variety of multilayer structures simply by adjusting the pH-sensitive linear charge density of the assembling polymers [37,55]. In-and-out diffusion of polyelectrolytes with coiled conformation (PAH at pH 7.5 and PAA at pH 3.5) leads to loose carbon nanotubes stacking along with voids and gaps between them. Such a randomly distributed nanotube structure in thicker polyelectrolytes layers impedes effective electrical transport, resulting in lower TE performances (as shown in Fig. 7, left). In comparison, the tight molecular chain packing and ordered DWNT structure observed at pH conditions corresponding to more extended polymeric conformation suggest the presence of highly interconnected conjugation network without nanotube aggregation. A continuous 3D nanostructure where conductive DWNT are in direct contact with each other above and

below layers is favorable to the charge carrier mobility (Fig. 7, right) [56]. Therefore, the interconnected architecture of DWNT in the thinner films provides efficient pathways for carrier transport that consequently enhances TE properties.

4. Conclusion

In this study, we demonstrated that manipulating assembly pH conditions of weak polyelectrolytes alters the growth behavior, structure, and mechanical properties by adjusting their conformation, which ultimately affects the thermoelectric performances of nanocomposites fabricated by the layer-by-layer technique. The 7.5PAH/3.5(DWNT-PAA) films grew rapidly due to thicker polymer morphology and in-and-out diffusion of weakly charged polyelectrolytes with coiled conformation. The exponentially-grown films yielded a maximum electrical conductivity of 24.7 S cm^{-1} and a Seebeck coefficient of 40 μV K^{-1} at 10 BL, translating to a power factor up to 3.95 μW m^{-1} K^{-2}. The TE performances were dramatically improved by tuning assembly pH conditions. The LbL thin films assembled with PAH at pH 6 and DWNT-PAA at pH 6.5 exhibited densely packed structures in which carbon nanotubes are uniformly deposited between the highly charged polyelectrolytes with extended molecular conformation. A 14 BL (~340 nm thick) 6PAH/6.5(DWNT-PAA) film achieved an electrical conductivity of 417 S cm^{-1} and a Seebeck coefficient of 85 μV K^{-1}, translating to a power factor of 301 μW m^{-1} K^{-2}, which is two orders of magnitude greater than that of the film made at PAH pH 7.5 and DWNT-PAA pH 3.5. The precise control of charge density with pH on polymer chain linearity, structure, and alignment of carbon nanofillers in the nanocomposites plays a crucial role in understanding morphology and tube-tube connection relationship as well as provides a potential route to boost the TE properties.

CRediT authorship contribution statement

You-young Byun: Conceptualization, Investigation, Data curation, Formal analysis. **Junho Jang:** Conceptualization, Investigation, Data curation, Formal analysis, Writing – original draft. **Mario Culebras:** Investigation, Formal analysis, Writing – review & editing. **Byeong-Soo Bae:** Investigation, Formal analysis, Writing – review & editing. **Jung Sang Cho:** Investigation, Formal analysis. **Yong Tae Park:** Supervision, Funding acquisition, Project administration. **Chungyeon Cho:** Supervision, Funding acquisition, Project administration.

Declaration of Competing Interest

The authors declare that they have no known competing financial interests or personal relationships that could have appeared to influence the work reported in this paper.

Acknowledgements

This research was supported by Wonkwang University in 2022.

Appendix A. Supplementary data

Supplementary data to this article can be found online at https://doi.org/10.1016/j.apsusc.2022.153483.

References

[1] D.K. Sam, W. Wang, S. Gong, E.K. Sam, X. Lv, J. Wang, J. Liu, Co2 Assisted Synthesis of Silk Fibroin Driven Robust N-Doped Carbon Aerogels Coupled with Nickel-Cobalt Particles as Highly Active Electrocatalysts for Her, Int. J. Hydrogen Energy 46 (2021) 21525–21533.
[2] C. Cho, K.L. Wallace, P. Tzeng, J.H. Hsu, C. Yu, J.C. Grunlan, Outstanding Low Temperature Thermoelectric Power Factor from Completely Organic Thin Films Enabled by Multidimensional Conjugated Nanomaterials, Adv. Energy Mater. 6 (2016) 1502168.
[3] K. Choi, J. Son, Y.T. Park, J.S. Cho, C. Cho, Effect of the Conformation Changes of Polyelectrolytes on Organic Thermoelectric Performances, Macromol. Res. 28 (2020) 997–1002.
[4] H.-G. Im, J. Jang, Y. Jeon, J. Noh, J. Jin, J.-Y. Lee, B.-S. Bae, Flexible Transparent Crystalline-Ito/Ag Nanowire Hybrid Electrode with High Stability for Organic Optoelectronics, ACS Appl. Mater. Interfaces 12 (2020) 56462–56469.
[5] K. Eom, Y.-E. Shin, J.-K. Kim, S.H. Joo, K. Kim, S.K. Kwak, H. Ko, J. Jin, S.J. Kang, Tailored Poly (Vinylidene Fluoride-Co-Trifluoroethylene) Crystal Orientation for a Triboelectric Nanogenerator through Epitaxial Growth on a Chitin Nanofiber Film, Nano Lett. 20 (2020) 6651–6659.
[6] J.-W. Jung, H.-G. Im, D. Lee, S. Yu, J.-H. Jang, K.R. Yoon, Y.H. Kim, J. B. Goodenough, J. Jin, I.-D. Kim, Conducting Nanopaper: A Carbon-Free Cathode Platform for Li–O2 Batteries, ACS Energy Lett. 2 (2017) 673–680.
[7] Y.J. Cui, B.L. Wang, K.F. Wang, Energy Conversion Performance Optimization and Strength Evaluation of a Wearable Thermoelectric Generator Made of a Thermoelectric Layer on a Flexible Substrate, Energy 229 (2021) 120694, https://doi.org/10.1016/j.energy.2021.120694.
[8] D. Kim, Y. Kim, K. Choi, J.C. Grunlan, C. Yu, Improved Thermoelectric Behavior of Nanotube-Filled Polymer Composites with Poly (3, 4-Ethylenedioxythiophene) Poly (Styrenesulfonate), ACS Nano 4 (1) (2010) 513–523.
[9] C. Cho, B. Stevens, J.H. Hsu, R. Bureau, D.A. Hagen, O. Regev, C. Yu, J.C. Grunlan, Completely Organic Multilayer Thin Film with Thermoelectric Power Factor Rivaling Inorganic Tellurides, Adv. Mater. 27 (2015) 2996–3001.
[10] N. Dubey, M. Leclerc, Conducting Polymers: Efficient Thermoelectric Materials, J. Polym. Sci., Part B: Polym. Phys. 49 (7) (2011) 467–475.
[11] S.I. Kim, K.H. Lee, H.A. Mun, H.S. Kim, S.W. Hwang, J.W. Roh, D.J. Yang, W. H. Shin, X.S. Li, Y.H. Lee, Dense Dislocation Arrays Embedded in Grain Boundaries for High-Performance Bulk Thermoelectrics, Science 348 (2015) 109–114.
[12] C. Han, G. Tan, T. Varghese, M.G. Kanatzidis, Y. Zhang, High-Performance Pbte Thermoelectric Films by Scalable and Low-Cost Printing, ACS Energy Lett. 3 (2018) 818–822.
[13] P.P. Murmu, S.V. Chong, J. Storey, S. Rubanov, J. Kennedy, Secondary phase induced electrical conductivity and improvement in thermoelectric power factor of zinc antimonide films, Mater. Today Energy 13 (2019) 249–255.
[14] P.P. Murmu, J. Kennedy, S. Suman, S.V. Chong, J. Leveneur, J. Storey, S. Rubanov, G. Ramanath, Multifold improvement of thermoelectric power factor by tuning bismuth and antimony in nanostructured n-type bismuth antimony telluride thin films, Mater. Des. 163 (2019), 107549.
[15] H. Jang, S. Abbey, W.H. Nam, B. Frimpong, C.V. Nguyen, S.-J. Joo, H.S. Shin, J. Y. Song, E.N. Cho, M. Kim, Order-Disorder Transition-Induced Band Nestification in Agbise 2–Cubise 2 Solid Solutions for Superior Thermoelectric Performance, J. Mater. Chem. A 9 (2021) 4648–4657.
[16] S. Peng, D. Wang, J. Lu, M. He, C. Xu, Y. Li, S. Zhu, A Review on Organic Polymer-Based Thermoelectric Materials, J. Polym. Environ. 25 (2017) 1208–1218.
[17] S. Kim, D.Y. Hyeon, S.S. Ham, J. Youn, H.S. Lee, S. Yi, K.T. Kim, K.-I. Park, Synergetic Enhancement of the Energy Harvesting Performance in Flexible Hybrid Generator Driven by Human Body Using Thermoelectric and Piezoelectric Combine Effects, Appl. Surf. Sci. 558 (2021) 149784, https://doi.org/10.1016/j.apsusc.2021.149784.
[18] F.F. Jaldurgam, Z. Ahmad, F. Touati, Synthesis and Performance of Large-Scale Cost-Effective Environment-Friendly Nanostructured Thermoelectric Materials, Nanomaterials 11 (2021) 1091.
[19] C. Yu, Y.S. Kim, D. Kim, J.C. Grunlan, Thermoelectric Behavior of Segregated-Network Polymer Nanocomposites, Nano Lett. 8 (2008) 4428–4432.
[20] A.D. Avery, B.H. Zhou, J. Lee, E.-S. Lee, E.M. Miller, R. Ihly, D. Wesenberg, K. S. Mistry, S.L. Guillot, B.L. Zink, Tailored Semiconducting Carbon Nanotube Networks with Enhanced Thermoelectric Properties, Nat. Energy 1 (2016) 1–9.
[21] J.L. Blackburn, A.J. Ferguson, C. Cho, J.C. Grunlan, Carbon-Nanotube-Based Thermoelectric Materials and Devices, Adv. Mater. 30 (2018) 1704386.
[22] Q. Jiang, J. Yang, P. Hing, H. Ye, Recent Advances, Design Guidelines, and Prospects of Flexible Organic/Inorganic Thermoelectric Composites, Mater. Adv. 1 (2020) 1038–1054.
[23] P. Goh, A. Ismail, B. Ng, Directional Alignment of Carbon Nanotubes in Polymer Matrices: Contemporary Approaches and Future Advances, Compos. A 56 (2014) 103–126.
[24] Z. Tang, Y. Wang, P. Podsiadlo, N.A. Kotov, Biomedical Applications of Layer-by-Layer Assembly: From Biomimetics to Tissue Engineering, Adv. Mater. 18 (2006) 3203–3224.
[25] X. Zhang, Y. Xu, X. Zhang, H. Wu, J. Shen, R. Chen, Y. Xiong, J. Li, S. Guo, Progress on the Layer-by-Layer Assembly of Multilayered Polymer Composites: Strategy, Structural Control and Applications, Prog. Polym. Sci. 89 (2019) 76–107.
[26] K. Ariga, Q. Ji, J.P. Hill, Y. Bando, M. Aono, Forming Nanomaterials as Layered Functional Structures toward Materials Nanoarchitectonics, NPG Asia Mater. 4 (5) (2012).
[27] K. Ariga, E. Ahn, M. Park, B.S. Kim, Layer-by-Layer Assembly: Recent Progress from Layered Assemblies to Layered Nanoarchitectonics, Chem. Asian J 14 (2019) 2553–2566.
[28] J. Zeng, M. Matsusaki, Layer-by-Layer Assembly of Nanofilms to Control Cell Functions, Polym. Chem. 10 (2019) 2960–2974.
[29] C. Cho, F. Xiang, K.L. Wallace, J.C. Grunlan, Combined Ionic and Hydrogen Bonding in Polymer Multilayer Thin Film for High Gas Barrier and Stretchiness, Macromolecules 48 (2015) 5723–5729.

[30] A.S. Ivanov, L.V. Pershina, K.G. Nikolaev, E.V. Skorb, Recent Progress of Layer-by-Layer Assembly, Free-Standing Film and Hydrogel Based on Polyelectrolytes, Macromol. Biosci. 21 (2021) 2100117.
[31] S. Nie, D. Jin, J.-N. Yang, G. Dai, Y. Luo, Fabrication of Environmentally-Benign Flame Retardant Cotton Fabrics with Hydrophobicity by a Facile Chemical Modification, Cellulose 26 (2019) 5147–5158.
[32] R.C. Hensel, M.A. Pereira-da-Silva, A. Riul, V. Rodrigues, Dielectric Permittivity and Surface Charge Density in Layer-by-Layer Poly (Diallyldimethylammonium Chloride)/Poly (Styrenesulfonate) Nanostructured Films: Implications for Biosensing, ACS Appl. Nano Mater. 3 (2) (2020) 1749–1754.
[33] O. Mermut, J. Lefebvre, D.G. Gray, C.J. Barrett, Structural and Mechanical Properties of Polyelectrolyte Multilayer Films Studied by Afm, Macromolecules 36 (2003) 8819–8824.
[34] C. Gayner, Y. Amouyal, Energy Filtering of Charge Carriers: Current Trends, Challenges, and Prospects for Thermoelectric Materials, Adv. Funct. Mater. 30 (2020) 1901789.
[35] P.P. Murmu, V. Karthik, Z. Liu, V. Jovic, T. Mori, W.L. Yang, K.E. Smith, J. V. Kennedy, Influence of Carrier Density and Energy Barrier Scattering on a High Seebeck Coefficient and Power Factor in Transparent Thermoelectric Copper Iodide, ACS Appl. Energy Mater. 3 (2020) 10037–10044.
[36] J. Kennedy, P.P. Murmu, P. Kumar, G. Ramanath, Multifold enhancements in thermoelectric power factor in isovalent sulfur doped bismuth antimony telluride films, Mater. Res. Bull. 142 (2021), 111426.
[37] S.S. Shiratori, M.F. Rubner, Ph-Dependent Thickness Behavior of Sequentially Adsorbed Layers of Weak Polyelectrolytes, Macromolecules 33 (2000) 4213–4219.
[38] J. Choi, M.F. Rubner, Influence of the Degree of Ionization on Weak Polyelectrolyte Multilayer Assembly, Macromolecules 38 (2005) 116–124.
[39] J. Mendelsohn, C.J. Barrett, V. Chan, A. Pal, A. Mayes, Rubner, MF, Fabrication of Microporous Thin Films from Polyelectrolyte Multilayers, Langmuir 16 (2000) 5017–5023.
[40] D. Bütergerds, C. Kateloe, C. Cramer, M. Schönhoff, Influence of the Degree of Ionization on the Growth Mechanism of Poly (Diallyldimethylammonium)/Poly (Acrylic Acid) Multilayers, J. Polym. Sci., Part B: Polym. Phys. 55 (5) (2017) 425–434.
[41] I. Choi, R. Suntivich, F.A. Plamper, C.V. Synatschke, A.H. Müller, V.V. Tsukruk, Ph-Controlled Exponential and Linear Growing Modes of Layer-by-Layer Assemblies of Star Polyelectrolytes, J. Am. Chem. Soc. 133 (2011) 9592–9606.
[42] Y.-H. Yang, M. Haile, Y.T. Park, F.A. Malek, J.C. Grunlan, Super Gas Barrier of All-Polymer Multilayer Thin Films, Macromolecules 44 (2011) 1450–1459.
[43] P. Podsiadlo, M. Michel, J. Lee, E. Verploegen, N. Wong Shi Kam, V. Ball, J. Lee, Y. Qi, A. J. Hart, P. T. Hammond, Exponential Growth of Lbl Films with Incorporated Inorganic Sheets. Nano Lett. 8 (2008) 1762-1770.
[44] C. Cho, K.L. Wallace, D.A. Hagen, B. Stevens, O. Regev, J.C. Grunlan, Nanobrick Wall Multilayer Thin Films Grown Faster and Stronger Using Electrophoretic Deposition, Nanotechnology 26 (2015), 185703.
[45] C. Cho, Y. Song, R. Allen, K.L. Wallace, J.C. Grunlan, Stretchable Electrically Conductive and High Gas Barrier Nanocomposites, J. Mater. Chem. C 6 (2018) 2095–2104.
[46] P.N. Nirmalraj, P.E. Lyons, S. De, J.N. Coleman, J.J. Boland, Electrical Connectivity in Single-Walled Carbon Nanotube Networks, Nano Lett. 9 (2009) 3890–3895.
[47] J. Jung, E.H. Suh, Y.J. Jeong, H.S. Yang, T. Lee, J. Jang, Efficient Debundling of Few-Walled Carbon Nanotubes by Wrapping with Donor-Acceptor Polymers for Improving Thermoelectric Properties, ACS Appl. Mater. Interfaces 11 (2019) 47330–47339.
[48] K. Biswas, J. He, I.D. Blum, C.-I. Wu, T.P. Hogan, D.N. Seidman, V.P. Dravid, M. G. Kanatzidis, High-Performance Bulk Thermoelectrics with All-Scale Hierarchical Architectures, Nature 489 (2012) 414–418.
[49] A.M. Glaudell, J.E. Cochran, S.N. Patel, M.L. Chabinyc, Impact of the Doping Method on Conductivity and Thermopower in Semiconducting Polythiophenes, Adv. Energy Mater. 5 (2015) 1401072.
[50] Y. Du, J. Xu, B. Paul, P. Eklund, Flexible Thermoelectric Materials and Devices, Appl. Mater. Today 12 (2018) 366–388.
[51] I. Petsagkourakis, E. Pavlopoulou, E. Cloutet, Y.F. Chen, X. Liu, M. Fahlman, M. Berggren, X. Crispin, S. Dilhaire, G. Fleury, Correlating the Seebeck Coefficient of Thermoelectric Polymer Thin Films to Their Charge Transport Mechanism, Org. Electron. 52 (2018) 335–341.
[52] D.L. Stevens, A. Parra, J.C. Grunlan, Thermoelectric Performance Improvement of Polymer Nanocomposites by Selective Thermal Degradation, ACS Appl. Energy Mater. 2 (2019) 5975–5982.
[53] S.L. Kim, K. Choi, A. Tazebay, C. Yu, Flexible Power Fabrics Made of Carbon Nanotubes for Harvesting Thermoelectricity, ACS Nano 8 (2014) 2377–2386.
[54] A. Kahn, Fermi Level, Work Function and Vacuum Level, Mater. Horiz. 3 (2016) 7–10.
[55] J.D. Mendelsohn, S.Y. Yang, J.A. Hiller, A.I. Hochbaum, M.F. Rubner, Rational Design of Cytophilic and Cytophobic Polyelectrolyte Multilayer Thin Films, Biomacromolecules 4 (2003) 96–106.
[56] Y. Liu, J. Zhao, Z. Li, C. Mu, W. Ma, H. Hu, K. Jiang, H. Lin, H. Ade, H. Yan, Aggregation and Morphology Control Enables Multiple Cases of High-Efficiency Polymer Solar Cells, Nat. Commun. 5 (2014) 1–8.